Int. J. Solids Structures, Vol. 34, No. 10, pp 1255-1281, 1996

STRESS TRANSFER INTO A FRAGMENTED, ANISOTROPIC FIBER THROUGH AN IMPERFECT INTERFACE

JOHN A. NAIRN and YUNG CHING LIU
Material Science and Engineering, University of Utah,
Salt Lake City, Utah 84112, U.S.A.

(*Received 9 September 1995; in revised form 3 April 1996*)

Abstract— A new analysis for stress transfer from the matrix to a fragmented fiber through an imperfect interface was derived using a Bessel-Fourier series stress function with some important additional polynomial terms. The solution satisfies equilibrium and compatibility every place and satisfies most boundary conditions exactly. The only approximation is that the axial stress in the fiber at a fiber break is equal to zero in an averaged sense instead of exactly. Two important advantages of the analysis are that it can handle anisotropic fibers and it can include imperfect interfaces or interphases. Theoretical predictions of stress transfer were compared to experimental Raman spectroscopy results. The results agreed well and were used to measure interface properties. The strain energy was integrated to get total strain energy in a fiber/matrix fragment. It is proposed that this result will be useful for developing fracture mechanics models of the fragmentation test.

INTRODUCTION

In the single-fiber fragmentation test (Wadsworth and Spilling (1968); Fraser *et al.* (1975); Drzal *et al.* (1983); Bascom and Jensen (1986); Bascom *et al.* (1991); Wagner *et al.* (1993)), a single fiber is embedded in a large amount of matrix and the specimen is loaded in tension until the fiber fragments. At the fiber breaks, the stress in the fiber is zero. As a function of position away from the break stress transfers back into the fiber from the matrix and across the fiber/matrix interface. The fiber fragmentation process is influenced by the efficiency of this stress transfer. The goal of the fragmentation test is to follow the fragmentation process and to use that information to extract information about interfacial properties.

For help in interpreting fragmentation test results, we have derived a new analysis for stress transfer into a fragmented fiber. The problem analyzed is illustrated in Fig. 1. Region R_1 is an anisotropic fiber fragment. It has a circular cross section of radius r_1 and a length of l. Region R_2 is an infinite, isotropic matrix. The matrix extends from $r = r_1$ to $r = \infty$ and has a length l. The boundary conditions on the fiber and matrix are

$$\sigma_{zz,1}(r, z = \pm l/2) = \tau_{rz,1}(r, z = \pm l/2) = \tau_{rz,2}(r, z = \pm l/2) = 0 \tag{1}$$

$$w_2(r, z = \pm l/2) = \pm \frac{l}{2}\left(\frac{\sigma_0}{E_m} + \alpha_m T\right) \tag{2}$$

where subscripts "1" and "2" refer to the fiber and matrix, respectively. The fiber axial and shear stresses, $\sigma_{zz,1}$ and $\tau_{rz,1}$, are zero at the fragment ends because the fiber is fragmented and the ends are the fracture surface. The matrix shear stresses, $\tau_{rz,2}$, are zero and the matrix displacement, w_2, is constant or is independent of r. These matrix boundary conditions are required to maintain compatibility of the stress state in one fragment with that of the adjacent fragment in the specimen. The constant matrix displacement is determined by the net strain on the infinite matrix. For the uniaxial loading used in fragmentation tests, the net strain is simply calculated from the applied stress, σ_0, the temperature differential, $T = T_s - T_0$ where T_s is the specimen temperature and T_0 is the stress-free temperature, and the modulus, E_m, and thermal expansion coefficient, α_m, of the matrix.

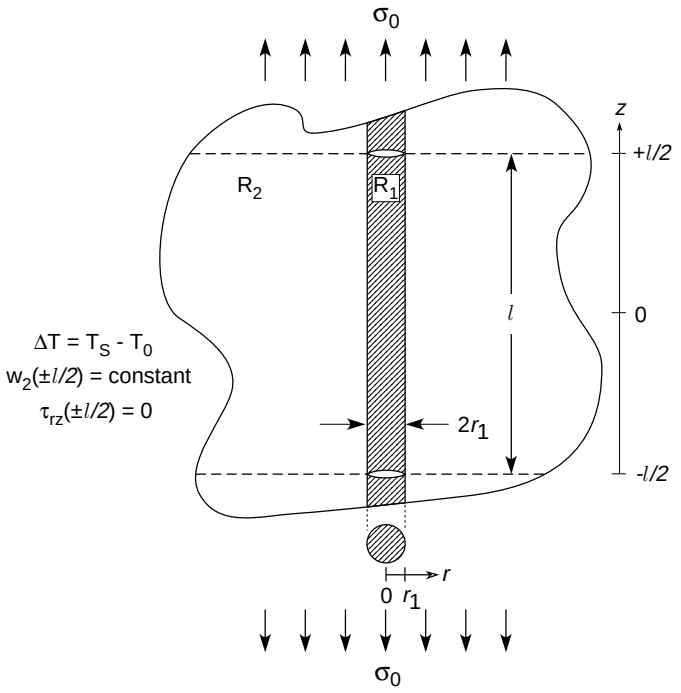

Fig. 1. A cross section of a single fiber fragment of length l and radius r_1 embedded in an infinite amount of matrix. The boundary conditions are indicated on the figure and described in the text of the paper (Note the σ_0 is the far-field matrix axial stress; the matrix axial stress at $\pm l/2$ is a function of r and a result of the analysis).

Many prior analyses of stress transfer assume a perfect interface between the fiber and the matrix (Muki and Sternberg (1969, 1970, 1971); Fowler and Sinclair (1978); Rajapakse and Shah (1987); Pak (1989); Pak and Gobert (1993); Slaughter and Sanders (1991); Nairn (1992); Kurtz and Pagano (1991)). Such analyses, however, are pointless when the goal is extract information about the interface. The process of interpreting fragmentation results can be described as solving an *inverse* problem. We observe the fragmentation process and attempt to deduce the input interfacial properties that led to those results. Clearly the stress analysis must include input interfacial properties. We included interfacial properties by using a simple *imperfect* interface model. At a perfect interface, all displacements must be continuous between the fiber and the matrix. For an imperfect interface we relaxed that requirement and allowed the displacements to be discontinuous. The magnitude of the discontinuities were assumed to be proportional to the magnitude of the interfacial stresses. The proportionality constants are the interfacial properties that influence the stress transfer process. Similar imperfect interface models have often been used to model imperfect interfaces (Martin (1992)). Hashin has specifically used displacement discontinuities to model the effect of the interface on the mechanical properties of a laminate (Hashin (1990); Hashin (1990)).

We thus considered the problem of stress transfer from a matrix to a fiber across an imperfect interface. There is a long literature of one-dimensional or shear-lag methods for studying stress transfer that originate with Cox (1952). Although these methods are still used today, one-dimensional models are not capable of giving explicit results about stress transfer. First, they always contain a "shear-lag" parameter which is unknown and which, in essence, determines the stress transfer rate. Second, they give no information on the radial terms in the stress state. Thus, when necessary, one-dimensional models must include assumptions about radial stress or about the radial redistribution of axial stress in the matrix. If these assumptions are not made correctly (and it is difficult to know how to make them), the one-dimensional models can be grossly in error (Nairn and Liu (1996)). Since 1970, many authors have abandoned one-dimensional models and sought three-dimensional, axisymmetric analyses for stress transfer from a rod or fiber into an elastic medium (Muki and Sternberg (1969, 1970, 1971); Fowler and Sinclair (1978); Rajapakse and Shah (1987); Pak (1989); Pak and Gobert (1993); Slaughter and Sanders (1991);

Nairn (1992); Kurtz and Pagano (1991)). In the composite field, these papers have concentrated on the single fiber pull-out test (Penn and Bowler (1981); Piggott *et al.* (1985)) where a fiber partially embedded in a matrix resin is pulled until it is pulled out of the matrix. In the civil engineering literature, the mathematically identically problem describes load transfer from a cylindrical foundation or pile into the surrounding earth (Fowler and Sinclair (1978); Rajapakse and Shah (1987); Pak (1989); Pak and Gobert (1993)). The first three-dimensional, axisymmetric analyses of stress transfer were for the pull-out geometry and were done by Muki and Sternberg (1969, 1970, 1971). They treated the matrix as a three-dimensional elastic continuum. The fiber was reduced to a fictitious, one-dimensional reinforcement over the cross section of the actual fiber. Although the Muki and Sternberg approach has been adopted in many subsequent papers (Fowler and Sinclair (1978); Rajapakse and Shah (1987); Pak (1989); Pak and Gobert (1993)), it is not ideal for analysis of the fragmentation test. First, the boundary conditions of the pull-out test and the fragmentation test are different. In particular, the surface of the matrix has zero *stress* in the pull-out test while it has constant *displacement* in the fragmentation test. Second, many fragmentation tests are done using anisotropic fibers such as carbon fibers. The reduction of the fiber to a one-dimensional reinforcement precludes the possibility of studying the effect of fiber anisotropy on the stress transfer process. Third, Muki and Sternberg assumed a perfect interface. Although an imperfect interface could be introduced into their model, we claim a more explicit treatment of the interface is warranted. Instead of blurring the fiber into a one-dimensional fictitious reinforcement, we treated the fiber as a three-dimensional, solid cylinder and modeled an imperfect interface by examining the stress state at the fiber/matrix interface.

We analyzed stress transfer in the fragmentation test using a stress-function approach based on a Bessel-Fourier series stress function. Several authors have previously used Bessel-Fourier series stress functions to solve stress transfer problems (Muki and Sternberg (1969); Kurtz and Pagano (1991); Parnes (1981)). They dealt with perfect interfaces, isotropic fibers, and boundary conditions different than the fragmentation test. We have adapted the Bessel-Fourier series approach to the fragmentation test and included the effects of an imperfect interface and anisotropic fibers. The Bessel-Fourier series alone cannot solve the fragmentation test. The key to the solution process is finding additional stress function terms to handle the boundary conditions. Kurtz and Pagano (1991) suggested some additional terms for the pull-out test. The additional terms appropriate for the fragmentation test, however, are different. We added some new polynomial terms and found a stress function that provides a nearly exact solution to the fragmentation problem. It obeys equilibrium and compatibility every place. It obeys all boundary conditions except one. The single approximation is that instead of the fiber axial stress being exactly zero at the fiber break, only the average axial fiber stress is equal to zero. After outlining the derivation of the stress analysis, the predictions are compared to direct experimental results of stress transfer done using Raman spectroscopy (Melanitis *et al.* (1993a)). The experiments and predictions agree well. Finally, we anticipate subsequent use of this stress analysis in fracture mechanics models. We thus evaluated the change in strain energy in a fiber/matrix fragment due to the presence of the fiber breaks and an imperfect interface.

STRESS ANALYSIS

The Stress Functions

We analyzed a single fragment from a fragmentation specimen as shown in Fig. 1. As illustrated in Fig. 2, the problem was partitioned into a far-field problem and a local field or perturbation problem. The far-field problem, illustrated in Fig. 2B, is for an infinitely long fiber embedded in an infinite matrix subjected to uniform axial stress and thermal load T. The boundary conditions for the far-field problem are:

$$\sigma_{zz,2}(r, z = \pm l/2) = \sigma_0 \tag{3}$$

$$\tau_{rz,1}(r, z = \pm l/2) = \tau_{rz,2}(r, z = \pm l/2) = 0 \tag{4}$$

$$w_1(r, z = \pm l/2) = w_2(r, z = \pm l/2) = \pm \frac{l}{2}\left(\frac{\sigma_0}{E_m} + \alpha_m T\right) \tag{5}$$

Realizing that the radial stresses at the interface must be continuous, the axisymmetric stresses for the far-field stresses have the form

$$\begin{array}{cccc} \sigma_{zz,1} = \psi_\infty & \sigma_{rr,1} = \sigma_\infty & \sigma_{\theta\theta,1} = \sigma_\infty & \tau_{rz,1} = 0 \\ \sigma_{zz,2} = \sigma_0 & \sigma_{rr,2} = \frac{r_1^2\sigma_\infty}{r^2} & \sigma_{\theta\theta,2} = -\frac{r_1^2\sigma_\infty}{r^2} & \tau_{rz,2} = 0 \end{array} \tag{6}$$

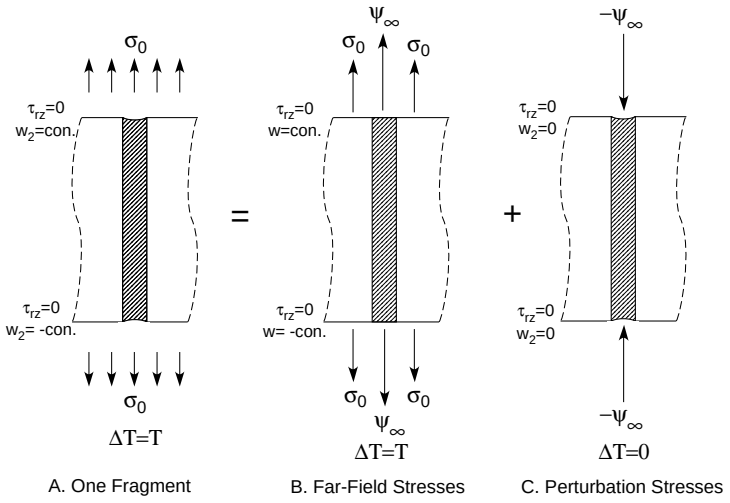

Fig. 2. The problem for stress transfer into a single fiber fragment (A) can be partitioned into the far-field stresses (B) and the local field or perturbation stresses (C). The far-field stresses are the stresses for an infinitely long, unbroken fiber in an infinite matrix under an applied stress of σ_0 and temperature differential of T. The perturbation stresses are the stresses for a fiber fragment loaded by compression stress of ψ_∞ while the matrix ends are maintained at zero displacement. The notation "con." means a constant that is independent of r.

By equating axial strains and the interfacial radial displacements, it is easy to show that the constants ψ_∞ and σ_∞ are

$$\psi_\infty = \frac{\left(\frac{2\nu_A\nu_m}{E_A} - \frac{1-\nu_T}{E_T} - \frac{1+\nu_m}{E_m}\right)\frac{E_A\sigma_0}{E_m} + \left(\frac{2\nu_A}{E_A}(\alpha_T-\alpha_m) + \left(\frac{1-\nu_T}{E_T} + \frac{1+\nu_m}{E_m}\right)(\alpha_A-\alpha_m)\right)E_AT}{\frac{2\nu_A^2}{E_A} - \frac{1-\nu_T}{E_T} - \frac{1+\nu_m}{E_m}} \tag{7}$$

$$\sigma_\infty = \frac{-(\nu_A-\nu_m)\frac{\sigma_0}{E_m} + \big(\nu_A(\alpha_A-\alpha_m) + (\alpha_T-\alpha_m)\big)T}{\frac{2\nu_A^2}{E_A} - \frac{1-\nu_T}{E_T} - \frac{1+\nu_m}{E_m}} \tag{8}$$

The anisotropic fiber is assumed to be transversely isotropic with the axial direction of symmetry coinciding with the axis of the fiber. The terms E_A, E_T, ν_A, ν_T, α_A, and α_T are the axial and transverse moduli, Poisson's ratios, and thermal expansion coefficients of the fiber. The matrix is assumed to be isotropic. The terms E_m, ν_m, and α_m are the modulus, Poisson's ratio, and thermal expansion coefficient of the matrix.

The challenging problem is the one for the perturbation stresses illustrated in Fig. 2C. The boundary conditions for the perturbation stresses are

$$\sigma_{zz,1}(r, z=\pm l/2) = -\psi_\infty \qquad \tau_{rz,1}(r, z=\pm l/2) = \tau_{rz,2}(r, z=\pm l/2) = 0 \qquad w_2(r, z=\pm l/2) = 0 \tag{9}$$

Because the temperature differential was already included in the far-field stresses, $T = 0$ for the perturbation stresses. We define $\vec{\sigma}_{0,i}$ as the far-field stresses in component i and $\vec{\sigma}_{p,i}$ as the perturbation stresses in component i due to unit compression on the fiber (due to $\sigma_{zz,1}(r, z=\pm l/2) = -1$). By superposition, the solution to the stresses in the fragment are $\vec{\sigma}_i = \vec{\sigma}_{0,i} + \psi_\infty\vec{\sigma}_{p,i}$. We need to find $\vec{\sigma}_{p,i}$.

From Lekhnitski (1981), the stresses and displacements for an axisymmetric stress state in a transversely isotropic fiber can be written as

$$\sigma_{rr} = -\frac{\partial}{\partial z}\left(\frac{\partial^2\Psi}{\partial r^2} + \frac{b}{r}\frac{\partial\Psi}{\partial r} + a\frac{\partial^2\Psi}{\partial z^2}\right) \tag{10}$$

$$\sigma_{\theta\theta} = -\frac{\partial}{\partial z}\left(b\frac{\partial^2\Psi}{\partial r^2} + \frac{1}{r}\frac{\partial\Psi}{\partial r} + a\frac{\partial^2\Psi}{\partial z^2}\right) \tag{11}$$

$$\sigma_{zz} = \frac{\partial}{\partial z}\left(c\frac{\partial^2\Psi}{\partial r^2} + \frac{c}{r}\frac{\partial\Psi}{\partial r} + d\frac{\partial^2\Psi}{\partial z^2}\right) \tag{12}$$

$$\tau_{rz} = \frac{\partial}{\partial r}\left(\frac{\partial^2\Psi}{\partial r^2}+\frac{1}{r}\frac{\partial\Psi}{\partial r}+a\frac{\partial^2\Psi}{\partial z^2}\right) \tag{13}$$

$$u = \frac{b-1}{2G_T}\frac{\partial^2\Psi}{\partial r\partial z} \tag{14}$$

$$w = \frac{1}{G_A}\left(\frac{\partial^2\Psi}{\partial r^2}+\frac{1}{r}\frac{\partial\Psi}{\partial r}\right)+\frac{(d+2\nu_A a)}{E_A}\frac{\partial^2\Psi}{\partial z^2} \tag{15}$$

where u is radial displacement and the constants are

$$a = \frac{-\nu_A(1+\nu_T)}{1-\frac{\nu_A^2 E_T}{E_A}} \tag{16}$$

$$b = \frac{\nu_T-\frac{\nu_A E_T}{E_A}\left(\frac{E_A}{G_A}-\nu_A\right)}{1-\frac{\nu_A^2 E_T}{E_A}} \tag{17}$$

$$c = \frac{\frac{E_A}{G_A}-\nu_A(1+\nu_T)}{1-\frac{\nu_A^2 E_T}{E_A}} \tag{18}$$

$$d = \frac{\frac{E_A}{2G_T}(1-\nu_T)}{1-\frac{\nu_A^2 E_T}{E_A}} \tag{19}$$

where G_A and G_T are the axial and transverse shear moduli. The stress function Ψ must satisfy the equation

$$\nabla_1^2\nabla_2^2\Psi = 0 \tag{20}$$

where the operators are defined by

$$\nabla_i^2 = \frac{\partial^2}{\partial r^2}+\frac{1}{r}\frac{\partial}{\partial r}+\frac{1}{s_i^2}\frac{\partial^2}{\partial z^2} \tag{21}$$

and the constants, s_1 and s_2 are

$$s_1^2 = \frac{a+c+\sqrt{(a+c)^2-4d}}{2d} \tag{22}$$

$$s_2^2 = \frac{a+c-\sqrt{(a+c)^2-4d}}{2d} \tag{23}$$

s_1 and s_2 may be either real or complex; they are never purely imaginary (Lekhnitski (1981)). For an isotropic material, these equations reduce to the well-known result in Love (1944):

$$\sigma_{rr} = \frac{\partial}{\partial z}\left(\nu_m\nabla^2\chi-\frac{\partial^2\chi}{\partial r^2}\right) \tag{24}$$

$$\sigma_{\theta\theta} = \frac{\partial}{\partial z}\left(\nu_m\nabla^2\chi-\frac{1}{r}\frac{\partial\chi}{\partial r}\right) \tag{25}$$

$$\sigma_{zz} = \frac{\partial}{\partial z}\left((2-\nu_m)\nabla^2\chi-\frac{\partial^2\chi}{\partial z^2}\right) \tag{26}$$

$$\tau_{rz} = \frac{\partial}{\partial r}\left((1-\nu_m)\nabla^2\chi-\frac{\partial^2\chi}{\partial z^2}\right) \tag{27}$$

$$u = -\frac{1}{2G}\frac{\partial^2\chi}{\partial r\partial z} \tag{28}$$

$$w = \frac{1}{2G}\left[2(1-\nu_m)\nabla^2\chi-\frac{\partial^2\chi}{\partial z^2}\right] \tag{29}$$

where $\chi = \Psi/(1-\nu)$ and the equation for χ is

$$\nabla^4\chi = 0 \tag{30}$$

It is well known that stress functions based on a Bessel-Fourier series can solve problems for a cylinder under arbitrary lateral loads (Love (1944)). Such functions are often used for analysis of isotropic materials, but they can also be used for anisotropic materials provided the material is transversely isotropic with the isotropic plane being normal to the cylinder axis (Lekhnitski (1981)). We thus begin by writing stress functions in the fiber and matrix as

$$\Psi = \sum_{i=1}^{\infty} \sin k_i z \big(b_{1i} I_0(\beta_{1i} r) + b_{2i} I_0(\beta_{2i} r)\big) \tag{31}$$

$$\chi = \sum_{i=1}^{\infty} \sin k_i z \left(a_{0i} K_0(k_i r) + a_{1i} k_i r K_1(k_i r)\right) \tag{32}$$

where

$$k_i = \frac{2i\pi}{l} \qquad \text{and} \qquad \beta_{ji} = \frac{k_i}{s_j} \tag{33}$$

The fiber stress function has modified Bessel functions of the first kind ($I_0(x)$); the matrix stress function has modified Bessel functions of the second kind ($K_0(x)$ and $K_1(x)$). The fiber has only modified Bessel functions of the first kind, because the second kind diverge as r approaches 0; the matrix has only modified Bessel functions of the second kind because the first kind diverge as r approaches ∞. The Fourier series include only $\sin k_i z$ terms due to symmetry about $z = 0$.

Substituting the fiber stress function in eqn (12), the axial stress in the fiber is

$$\sigma_{zz} = \sum_{i=1}^{\infty} k_i^3 \cos k_i z \left[b_{1i} \left(\frac{c}{s_1^2} - d \right) I_0(\beta_{1i} r) + b_{2i} \left(\frac{c}{s_2^2} - d \right) I_0(\beta_{2i} r) \right] \tag{34}$$

This result is insufficiently general to solve the fragmentation problem. It expands the axial stress in a Fourier series. It correctly includes only $\cos k_i z$ terms because the axial stress is an even function of z. But, it does not have a constant term or a Fourier term for $i = 0$. To correct this deficiency of the Bessel-Fourier series stress function, we must superpose it with some additional stress functions. Our goal is to recover the z-independent terms while still satisfying boundary and symmetry conditions. We looked to the polynomial stress functions for transversely isotropic materials given in Lekhnitski (1981):

$$\Psi_m = A_{m0} z + A_{m2} r^2 z^{m-2} + \dots \tag{35}$$

First, m must be odd, because even m leads to normal stresses that are odd functions of z rather than the required even functions. Among the odd-m functions, Ψ_1 trivially gives zero stress and Ψ_7 and higher always give non-zero shear stresses at $z = \pm l/2$. We are left with Ψ_3 and Ψ_5 which have the form

$$\Psi_3 = A_{30} z^3 + A_{32} r^2 z \qquad \text{and} \qquad \Psi_5 = A_{50} \left(z^5 - \frac{15}{8} d r^4 z \right) + A_{52} \left(r^2 z^3 - \frac{3}{8}(a + c) r^4 z \right) \tag{36}$$

Substituting these stresses into eqn (13) we find zero shear stress at $z = \pm l/2$ for arbitrary values of A_{30}, A_{32}, and A_{50}, but the remaining constant must be

$$A_{52} = -\frac{5d}{c} A_{50} \tag{37}$$

Combining the polynomial stress functions with the Bessel-Fourier series stress function, the total perturbation stress function for the fiber becomes

$$\Psi = A_{30} z^3 + A_{32} r^2 z + \frac{A_{50}}{c} \left(c z^5 + \frac{15ad}{8} r^4 z - 5 d r^2 z^3 \right) + \sum_{i=1}^{\infty} \sin k_i z \big(b_{1i} I_0(\beta_{1i} r) + b_{2i} I_0(\beta_{2i} r)\big) \tag{38}$$

The situation is similar for the matrix stress function. By using separation of variables, it is easy to show that

$$\phi = A_1 z \ln r + A_2 \ln r + A_3 z + A_4 \tag{39}$$

is a solution to $\nabla^2\phi = 0$ and therefore an acceptable stress function for the matrix. Inserting ϕ in eqns (24)–(29) gives the required z-independent stresses; the stresses are also compatible with the boundary conditions of the fragmentation problem. Furthermore only the A_1 term enters the stresses that result from ϕ. We tried other matrix stress functions, but could not find any that are similarly compatible with the boundary conditions. Combining the A_1 term in ϕ with the Bessel-Fourier series stress function, the total perturbation stress function for the matrix becomes

$$\chi = A_1 z \ln r + \sum_{i=1}^{\infty} \sin k_i z \left(a_{0i} K_0(k_i r) + a_{1i} k_i r K_1(k_i r)\right) \tag{40}$$

To find and stress or displacement in the fiber or matrix, we substitute the fiber or matrix stress function into the required equation among eqns (10)–(15) or eqns (24)–(29). The strains can be calculated from the stresses. Here we explicitly state only those stresses, strains, or displacements that are necessary for solving the stress transfer problem — the axial, shear, and radial stresses, the axial strain, and the axial and radial displacements in both the fiber and the matrix:

$$\sigma_{zz,1} = B_2 + B_3 d\xi^2 + \sum_{i=1}^{\infty} \cos k_i\zeta \left[b_{1i} \left(\frac{c}{s_1^2} - d \right) I_0(\beta_{1i}\xi) + b_{2i} \left(\frac{c}{s_2^2} - d \right) I_0(\beta_{2i}\xi) \right] \tag{41}$$

$$\tau_{rz,1} = \sum_{i=1}^{\infty} \sin k_i\zeta \left[b_{1i} \left(\frac{1}{s_1^2} - a \right) \frac{I_1(\beta_{1i}\xi)}{s_1} + b_{2i} \left(\frac{1}{s_2^2} - a \right) \frac{I_1(\beta_{2i}\xi)}{s_2} \right] \tag{42}$$

$$\begin{aligned} \sigma_{rr,1} = {} & B_1 - B_3 \left[\frac{(1+\nu_T)\rho^2}{3} + \frac{(1-\nu_T)a}{4}\xi^2 \right] + \sum_{i=1}^{\infty} \cos k_i\zeta \left[-B_3(-1)^i \frac{4(1+\nu_T)}{k_i^2} + b_{1i} \left(\left(a - \frac{1}{s_1^2} \right) I_0(\beta_{1i}\xi) \right.\right. \\ & \left.\left. + \frac{(1-b)}{s_1^2} \frac{I_1(\beta_{1i}\xi)}{\beta_{1i}\xi} \right) + b_{2i} \left(\left(a - \frac{1}{s_2^2} \right) I_0(\beta_{2i}\xi) + \frac{(1-b)}{s_2^2} \frac{I_1(\beta_{2i}\xi)}{\beta_{2i}\xi} \right) \right] \end{aligned} \tag{43}$$

$$\begin{aligned} w_1 = {} & \zeta \left(\frac{1}{E_A} B_2 - \frac{2\nu_A}{E_A} B_1 \right) + \frac{B_3}{2G_T} \left[(1-\nu_T)\xi^2\zeta + \frac{2\nu_A E_T \rho^2}{3E_A}\zeta \right] + \sum_{i=1}^{\infty} \frac{\sin k_i\zeta}{k_i} \left[B_3(-1)^i \frac{8\nu_A(1+\nu_T)}{E_A k_i^2} \right. \\ & \left. + b_{1i} \left(\frac{1}{s_1^2 G_A} - \frac{d + 2\nu_A a}{E_A} \right) I_0(\beta_{1i} r) + b_{2i} \left(\frac{1}{s_2^2 G_A} - \frac{d + 2\nu_A a}{E_A} \right) I_0(\beta_{2i} r) \right] \end{aligned} \tag{44}$$

$$\begin{aligned} \varepsilon_{zz,1} = {} & \frac{\partial w_1}{\partial \zeta} = -\frac{2\nu_A}{E_A} B_1 + \frac{1}{E_A} B_2 + \frac{B_3}{2G_T} \left[(1-\nu_T)\xi^2 + \frac{2\nu_A E_T \rho^2}{3E_A} \right] + \sum_{i=1}^{\infty} \cos k_i\zeta \left[B_3(-1)^i \frac{8\nu_A(1+\nu_T)}{E_A k_i^2} \right. \\ & \left. + b_{1i} \left(\frac{1}{s_1^2 G_A} - \frac{d + 2\nu_A a}{E_A} \right) I_0(\beta_{1i}\xi) + b_{2i} \left(\frac{1}{s_2^2 G_A} - \frac{d + 2\nu_A a}{E_A} \right) I_0(\beta_{2i}\xi) \right] \end{aligned} \tag{45}$$

$$\begin{aligned} u_1 = {} & \xi \left(\frac{1-\nu_T}{E_T} B_1 - \frac{\nu_A}{E_A} B_2 \right) + \frac{B_3(1-\nu_T)}{2G_T} \left(\frac{a\xi^3}{4} - \frac{\xi\rho^2}{3} \right) + \frac{1}{2G_T} \sum_{i=1}^{\infty} \cos k_i\zeta \left[-B_3(-1)^i \frac{4(1-\nu_T)\xi}{k_i^2} \right. \\ & \left. + \frac{b_{1i}(b-1)}{s_1^2} \frac{I_1(\beta_{1i}\xi)}{\beta_{1i}} + \frac{b_{2i}(b-1)}{s_2^2} \frac{I_2(\beta_{2i}\xi)}{\beta_{2i}} \right] \end{aligned} \tag{46}$$

$$\sigma_{zz,2} = \sum_{i=1}^{\infty} \cos k_i\zeta \left[a_{0i} K_0(k_i\xi) + a_{1i} \big(k_i\xi K_1(k_i\xi) - 2(2-\nu_m) K_0(k_i\xi) \big) \right] \tag{47}$$

$$\tau_{rz,2} = \sum_{i=1}^{\infty} \sin k_i\zeta \left[a_{0i} \left(-K_1(k_i\xi) \right) + a_{1i} \big(2(1-\nu_m) K_1(k_i\xi) - k_i\xi K_0(k_i\xi) \big) \right] \tag{48}$$

$$\sigma_{rr,2} = \frac{A_1}{\xi^2} + \sum_{i=1}^{\infty} \cos k_i\zeta \left[a_{0i} \left(-K_0(k_i\xi) - \frac{K_1(k_i\xi)}{k_i\xi} \right) + a_{1i} \big((1-2\nu_m) K_0(k_i\xi) - k_i\xi K_1(k_i\xi) \big) \right] \tag{49}$$

$$w_2 = \frac{1}{2G_m} \sum_{i=1}^{\infty} \frac{\sin k_i\zeta}{k_i} \left[a_{0i} K_0(k_i\xi) + a_{1i} \big(k_i\xi K_1(k_i\xi) - 4(1-\nu_m) K_0(k_i\xi) \big) \right] \tag{50}$$

$$\varepsilon_{zz,2} = \frac{\partial w_2}{\partial \zeta} = \frac{1}{2G_m}\sum_{i=1}^{\infty}\cos k_i\zeta\left[a_{0i}K_0(k_i\xi) + a_{1i}\big(k_i\xi K_1(k_i\xi) - 4(1-\nu_m)K_0(k_i\xi)\big)\right] \quad (51)$$

$$u_2 = -\frac{1}{2G_m}\frac{A_1}{\xi} + \frac{1}{2G_m}\sum_{i=1}^{\infty}\cos k_i\zeta\left(a_{0i}\frac{K_1(k_i\xi)}{k_i} + a_{1i}\xi K_0(k_i\xi)\right) \quad (52)$$

In deriving these results we additionally transformed to a dimensionless coordinate system with $\xi = r/r_1$ and $\zeta = z/r_1$. This change required a redefinition of k_i to be

$$k_i = \frac{2r_1 i\pi}{l} = \frac{i\pi}{\rho} \quad (53)$$

where $\rho = l/(2r_1)$ is the aspect ratio of the fragment. For simplicity we have defined some new constants (B_1, B_2, and B_3) to replace the previous constants A_{30}, A_{32}, and A_{50}. We also redefined the remaining constants (A_1, a_{0i}, a_{1i}, b_{1i}, and b_{2i}) to eliminate some unnecessary common factors. The total number of undetermined constants is unchanged. Finally, we note that the displacements u_i and w_i are dimensionless displacements that are normalized by the fiber radius; for example, $u_1 = u_1(\text{actual})/r_1$.

Special mention needs to be made about the Fourier expansion terms in the radial stress, axial strain, and radial displacement in the fiber. Each of these terms includes two Bessel-function terms and a third non-Bessel function term involving B_3. The non-Bessel function terms in the Fourier expansion arise from the leading terms in the fiber stress function. For example, the radial stress due to only the leading terms in the fiber stress function is

$$\sigma_{rr,1} = B_1 - B_3\left[(1+\nu_T)\zeta^2 + \frac{(1-\nu_T)a}{4}\xi^2\right] \quad (54)$$

As discussed above, this radial stress furnishes the desired component that is independent of ζ, but it also has a component that varies as ζ^2. Our subsequent analysis will do a term-by-term comparison between two Fourier expansions. For this method to work, both sides of the equation *must* be completely resolved into its Fourier terms. For terms involving ζ^2, we thus introduce the Fourier expansion

$$\zeta^2 = \frac{\rho^2}{3} + \sum_{i=1}^{\infty}(-1)^i\frac{4}{k_i^2}\cos k_i\zeta \quad (55)$$

The constant parts are kept with the ζ-independent parts of the stresses, strains, and displacement. The Fourier parts are added to the Fourier expansion terms. The non-Bessel function terms in the Fourier expansion are crucial to the analysis. Without them, the interface conditions described below would yield only a trivial result of zero perturbation stress. With them, a useful solution to the stress transfer problem is possible.

In the dimensionless coordinates, the fiber fragment extends from $-\rho$ to ρ. Inspection of the matrix shear stress, the matrix axial displacement, and the fiber shear stress show that

$$\tau_{rz,2}(\pm\rho) = 0 \qquad w_2(\pm\rho) = 0 \qquad \tau_{rz,1}(\pm\rho) = 0 \quad (56)$$

Thus the stress state automatically satisfies three of the four boundary conditions in eqn (9). The remaining boundary condition is $\sigma_{zz,1}(\pm\rho) = -1$. Because $\sigma_{zz,1}(\pm\rho)$ in eqn (41) is a function of ξ, this final boundary condition cannot be satisfied exactly. Instead, we satisfy it in the average or we satisfy $\langle\sigma_{zz,1}(\pm\rho)\rangle = -1$. Integrating $\sigma_{zz,1}$ over the cross-section gives the average axial stress in the fiber:

$$\langle\sigma_{zz,1}\rangle = B_2 + \frac{B_3 d}{2} + \sum_{i=1}^{\infty}\cos k_i\zeta\left[b_{1i}\left(\frac{c}{s_1^2} - d\right)\frac{I_1(\beta_{1i})}{\beta_{1i}} + b_{2i}\left(\frac{c}{s_2^2} - d\right)\frac{I_1(\beta_{2i})}{\beta_{2i}}\right] \quad (57)$$

We thus replace the $\sigma_{zz,1}(\pm\rho) = -1$ boundary condition with $\langle\sigma_{zz,1}(\pm\rho)\rangle = -1$ or explicitly with

$$-1 = B_2 + \frac{B_3 d}{2} + 2\sum_{i=1}^{\infty}(-1)^i\left[b_{1i}\left(\frac{c}{s_1^2} - d\right)\frac{I_1(\beta_{1i})}{\beta_{1i}} + b_{2i}\left(\frac{c}{s_2^2} - d\right)\frac{I_1(\beta_{2i})}{\beta_{2i}}\right] \quad (58)$$

Unfortunately, the results for isotropic fibers are not a special case of the above results for anisotropic fibers. The difficulty is that for isotropic fibers $s_1 = s_2 = 1$ and the two Bessel function terms become degenerate. The solution is to add a new Bessel function term that depends on $I_1(k_i r)$ instead of $I_0(k_i r)$ (Love (1944)). The stress function for isotropic fibers, complete with leading terms, is

$$\Psi = A_{30} z^3 + A_{32} r^2 z + A_{50} \left((2-\nu_f) z^5 - \frac{15\nu_f}{8} r^4 z - 5(1-\nu_f) r^2 z^3 \right) + \sum_{i=1}^{\infty} \sin k_i z \big(b_{1i} I_0(k_i r) + b_{2i} k_i r I_1(k_i r) \big) \tag{59}$$

where ν_f is the Poisson's ratio of the isotropic fiber. The leading terms are the same as the leading terms for anisotropic fibers after inserting the special case of isotropic material properties. Substituting this stress function into eqns (24)–(29), the required results for isotropic fibers are:

$$\sigma_{zz,1} = B_2 + B_3 \xi^2 + \sum_{i=1}^{\infty} \cos k_i \zeta \left[b_{0i} I_0(k_i \xi) + b_{1i} \big(k_i \xi I_1(k_i \xi) + 2(2-\nu_f) I_0(k_i \xi) \big) \right] \tag{60}$$

$$\tau_{rz,1} = \sum_{i=1}^{\infty} \sin k_i \zeta \left[b_{0i} I_1(k_i \xi) + b_{1i} \big(2(1-\nu_f) I_1(k_i \xi) + k_i \xi I_0(k_i \xi) \big) \right] \tag{61}$$

$$\begin{aligned} \sigma_{rr,1} = {} & B_1 - B_3 \left[\frac{(1+\nu_f)\rho^2}{3} - \frac{\nu_f}{4} \xi^2 \right] + \sum_{i=1}^{\infty} \cos k_i \zeta \Bigg[-B_3 (-1)^i \frac{4(1+\nu_f)}{k_i^2} \\ & + b_{0i} \left(-I_0(k_i \xi) + \frac{I_1(k_i \xi)}{k_i \xi} \right) + b_{1i} \big(-(1-2\nu_f) I_0(k_i \xi) - k_i \xi I_1(k_i \xi) \big) \Bigg] \end{aligned} \tag{62}$$

$$\begin{aligned} w_1 = {} & \zeta \left(\frac{1}{E_f} B_2 - \frac{2\nu_f}{E_f} B_1 \right) + \frac{B_3}{2G_f} \left[(1-\nu_f) \xi^2 \zeta + \frac{2\nu_f \rho^2}{3} \zeta \right] + \frac{1}{2G_f} \sum_{i=1}^{\infty} \frac{\sin k_i \zeta}{k_i} \Big[B_3 (-1)^i \frac{8\nu_f}{k_i^2} \\ & + b_{0i} I_0(k_i \xi) + b_{1i} \big(k_i \xi I_1(k_i \xi) + 4(1-\nu_f) I_0(k_i \xi) \big) \Big] \end{aligned} \tag{63}$$

$$\begin{aligned} \varepsilon_{zz,1} = {} & -\frac{2\nu_f}{E_f} B_1 + \frac{1}{E_f} B_2 + \frac{B_3}{2G_f} \left[(1-\nu_f) \xi^2 + \frac{2\nu_f \rho^2}{3} \right] + \frac{1}{2G_f} \sum_{i=1}^{\infty} \cos k_i \zeta \Bigg[B_3 (-1)^i \frac{8\nu_f}{k_i^2} \\ & + b_{0i} I_0(k_i \xi) + b_{1i} \big(k_i \xi I_1(k_i \xi) + 4(1-\nu_f) I_0(k_i \xi) \big) \Bigg] \end{aligned} \tag{64}$$

$$\begin{aligned} u_1 = {} & \xi \left(\frac{1-\nu_f}{E_f} B_1 - \frac{\nu_f}{E_f} B_2 \right) - \frac{B_3}{2G_f} \left(\frac{\nu_f \xi^3}{4} + \frac{(1-\nu_f)\xi \rho^2}{3} \right) \\ & + \frac{1}{2G_f} \sum_{i=1}^{\infty} \cos k_i \zeta \left[-B_3 (-1)^i \frac{4(1-\nu_f)\xi}{k_i^2} - b_{0i} \frac{I_1(k_i \xi)}{k_i} - b_{1i} \xi I_0(k_i \xi) \right] \end{aligned} \tag{65}$$

where E_f and G_f are the Young's and shear moduli of the fiber. The average axial fiber stress becomes

$$\langle \sigma_{zz,1} \rangle = B_2 + \frac{B_3}{2} + 2 \sum_{i=1}^{\infty} \cos k_i \zeta \left[b_{1i} \frac{I_1(k_i)}{k_i} + b_{2i} \left(I_0(k_i) + 2(1-\nu_f) \frac{I_1(k_i)}{k_i} \right) \right] \tag{66}$$

Imperfect Interface

The stresses, strains, and displacements in the previous section depend on numerous undetermined constants. Those constants can all be determined by imposing conditions on the fiber/matrix interface. In analyses that assume a perfect interface, σ_{rr}, τ_{rz}, u, and w are all continuous at $r = r_1$ or at $\xi = 1$. The goal of the fragmentation test, however, is to assess the role of the interface in the stress transfer process. It is self-evident that analyses that assume a perfect interface will never be helpful in interpreting such tests. Those analyses predetermine the role of the interface; they include no interface property that can influence stress transfer. To use stress analysis to study interfaces, we *must* include some model for an imperfect interface into the stress analysis.

The mathematician's approach to an imperfect interface is to relax interfacial continuity conditions and allow there to be discontinuities in σ_{rr}, τ_{rz}, u, and w (Martin (1992)). In linear theories, the discontinuities are assumed to be linear functions of the interfacial stress state. In static loading conditions, stress equilibrium requires σ_{rr} and τ_{rz} to be continuous regardless of the quality of the interface. The remaining discontinuities in u and w are functions of the interfacial stresses. Hashin put this imperfect interface model into physical terms for composites (Hashin (1990); Hashin (1990)). The interface in real composites is better described as an interface zone of finite dimension or an *interphase*. Within the interphase, the mechanical properties differ from both the fiber and the matrix. If the interphase plays a role in composite properties, then it must allow the fiber to displace relative to the matrix. Unfortunately, we are unlikely to have detailed information about the thickness or the mechanical properties of the interphase. To make matters more complex, there might be a gradient of mechanical properties across the interphase. Adding an interphase zone with variable and probably unknown mechanical properties severely complicates any analysis. Hashin proposed collapsing the 3D interphase into a 2D interface (Hashin (1990); Hashin (1990)). The effect of the interphase is modeled by allowing displacement discontinuities at the 2D interface that are linearly related to the stress in each displacement direction. Denoting interface discontinuities with square brackets (*e.g.*, $[u] = u_2(1,\zeta) - u_1(1,\zeta)$), a fiber interface reduces to

$$[u] = \frac{\sigma_{rr,1}(1,\zeta)}{D_n} = \frac{\sigma_{rr,2}(1,\zeta)}{D_n} \tag{67}$$

$$[w] = \frac{\tau_{rz,1}(1,\zeta)}{D_s} = \frac{\tau_{rz,2}(1,\zeta)}{D_s} \tag{68}$$

$$[v] = \frac{\tau_{r\theta,1}(1,\zeta)}{D_t} = \frac{\tau_{r\theta,2}(1,\zeta)}{D_t} \tag{69}$$

where D_n, D_s, and D_t are called interface parameters. They express the ability of the interphase to transfer stress. A perfect interface is described by $D_n = D_s = D_t = \infty$; a completely disbonded interface is described by $D_n = D_s = D_t = 0$; intermediate values describe an imperfect interface or a partially debonded interface.

Fortunately, the number of interface parameters required for the fragmentation test can be reduced. First, the stresses are axisymmetric which implies $\tau_{r\theta} = [v] = 0$; we do not need to consider D_t. Second, in the fragmentation test, thermal shrinkage of the matrix and differential Poisson's contraction between the fiber and the matrix both promote compressive radial stresses (Nairn (1992)). Calculation of $\sigma_{rr}(1,\zeta)$ from the above stress analysis confirms that σ_{rr} is compressive over the entire interface except for extremely small zones near the fiber ends. Under dominantly compressive radial stresses, the expression for $[u]$ implies a negative discontinuity or implies the matrix penetrates into the fiber. While negative discontinuities are permissible for tangential displacement, they should be forbidden for normal displacements. We can prevent negative discontinuities in normal displacements by setting $D_n = \infty$. We are not assuming the interface is perfect in the radial direction; we are just exploiting the fact that σ_{rr} is compressive and therefore the quality of the interface in the radial direction should have no effect on fragmentation results. The remaining interface parameter, D_s, cannot be eliminated. Thus we claim the effect of an imperfect interface on stress transfer in the fragmentation test can be modeled with a single parameter — D_s.

Collapsing the interphase to a 2D interface does not mean we are ignoring the reality of an interphase. Instead, we are using a mathematical trick that lumps the effect of the interphase into one interface parameter — D_s. In principle, D_s could be calculated for an interphase if its mechanical properties and dimensions were known. Some sample calculations for planar interfaces are given in Martin (1992). For the fragmentation test, consider a compliant interphase of thickness t_i on a fiber. The discontinuity in axial displacement across the interphase is $r_1[w]$ (when w is a dimensionless displacement). A simple one-dimensional analysis for shear strain in the interphase gives

$$\gamma_{xz,i} = \frac{r_1[w]}{t_i} \tag{70}$$

Substituting the imperfect interface model for $[w]$ and assuming the interphase shear stiffness is G_i we find a physical interpretation for D_s as

$$D_s = \frac{r_1 G_i}{t_i} \tag{71}$$

Thus D_s has units of a modulus and is related to the *effective* shear stiffness of the interphase. This one-dimensional picture probably oversimplifies the physical meaning of D_s. D_s is better imagined as a measure of the ability of the interphase to transfer stress from the matrix back into the fiber.

The Unknown Constants

The conditions available for determining the unknown constants are

$$\sigma_{rr,1}(1,\zeta) = \sigma_{rr,2}(1,\zeta) \tag{72}$$
$$\tau_{rz,1}(1,\zeta) = \tau_{rz,2}(1,\zeta) \tag{73}$$
$$[u] = 0 \tag{74}$$
$$[w] = \frac{\tau_{rz,1}(1,\zeta)}{D_s} \tag{75}$$
$$\langle \sigma_{zz,1}(\pm\rho)\rangle = -1 \tag{76}$$

The first four are the interface conditions; the inclusion of D_s is the effect of the imperfect interface. The last condition is the average stress on the fiber ends. The axial displacement discontinuity is more conveniently expressed in terms of axial strains. Using

$$[w] = \int_0^{\zeta} \big(\varepsilon_{zz,2} - \varepsilon_{zz,1}\big) d\zeta, \tag{77}$$

the axial displacement discontinuity condition can be rewritten as

$$\varepsilon_{zz,2} - \varepsilon_{zz,1} = \frac{1}{D_s} \frac{\partial \tau_{rz,1}(1,\zeta)}{\partial \zeta} \tag{78}$$

To solve for the unknown constants, we first define some new constants:

$$c_{1i} = \frac{b_{1i}}{B_3} \qquad c_{2i} = \frac{b_{2i}}{B_3} \qquad c_{3i} = \frac{a_{0i}}{B_3} \qquad c_{4i} = \frac{a_{1i}}{B_3} \tag{79}$$

Introducing these constants into the four interface conditions and equating the $\cos k_i\xi$ terms for $i = 1$ to n, where n is the number of Fourier terms, results in n (4×4) linear systems for c_{1i}, c_{2i}, c_{3i}, and c_{3i}. In matrix form the linear systems are

$$\begin{pmatrix} \left(a - \frac{1}{s_1^2}\right)\frac{I_1(\beta_{1i})}{s_1} & \left(a - \frac{1}{s_2^2}\right)\frac{I_1(\beta_{2i})}{s_2} & -K_1(k_i) \\ \left(a - \frac{1}{s_1^2}\right) I_0(\beta_{1i}) + \frac{(1-b)}{s_1^2}\frac{I_1(\beta_{1i})}{\beta_{1i}} & \left(a - \frac{1}{s_2^2}\right) I_0(\beta_{2i}) + \frac{(1-b)}{s_2^2}\frac{I_1(\beta_{2i})}{\beta_{2i}} & K_0(k_i) + \frac{K_1(k_i)}{k_i} \\ \frac{(b-1)}{s_1^2}\frac{I_1(\beta_{1i})}{2G_T\beta_{1i}} & \frac{(b-1)}{s_2^2}\frac{I_1(\beta_{2i})}{2G_T\beta_{2i}} & -\frac{K_1(k_i)}{2G_m k_i} \\ -\left(\frac{1}{s_1^2 G_A} - \frac{d+2\nu_A a}{E_A}\right) I_0(\beta_{1i}) & -\left(\frac{1}{s_2^2 G_A} - \frac{d+2\nu_A a}{E_A}\right) I_0(\beta_{2i}) & \frac{K_0(k_i)}{2G_m} \\ -\left(\frac{1}{s_1^2} - a\right)\frac{\beta_{1i} I_1(\beta_{1i})}{D_s} & -\left(\frac{1}{s_2^2} - a\right)\frac{\beta_{2i} I_1(\beta_{2i})}{D_s} & \end{pmatrix}$$

$$\begin{pmatrix} 2(1-\nu_m)K_1(k_i) - k_i K_0(k_i) \\ -(1-2\nu_m)K_0(k_i) + k_i K_1(k_i) \\ -\frac{K_0(k_i)}{2G_m} \\ \frac{1}{2G_m}\big(k_i K_1(k_i) - 4(1-\nu_m)K_0(k_i)\big) \end{pmatrix} \begin{pmatrix} c_{1i} \\ c_{2i} \\ c_{3i} \\ c_{4i} \end{pmatrix} = \begin{pmatrix} 0 \\ (-1)^i \frac{4(1+\nu_T)}{k_i^2} \\ (-1)^i \frac{4(1-\nu_T)}{2G_T k_i^2} \\ (-1)^i \frac{8\nu_A(1+\nu_T)}{E_A k_i^2} \end{pmatrix} \tag{80}$$

Note the the right-hand side of this equation contains the Fourier terms that resulted from expanding the ζ^2 terms in the stresses that resulted from the leading terms in the fiber stress function. Without these terms, the right-hand side would be zero and only the trivial solution of $c_{1i} = c_{2i} = c_{3i} = c_{4i} = 0$ would be possible. With them a nonzero solution is possible. Thus we see the importance of the leading terms in the fiber and matrix stress functions.

Once c_{1i}, c_{2i}, c_{3i}, and c_{4i} are determined, we use the ζ-independent terms to find A_1, B_1, B_2, and B_3. We get three equations from the interfacial conditions on radial stress, radial displacement, and axial strain.

The interfacial shear stress condition, however, has no ζ-independent terms. The required fourth equation comes from the $\langle\sigma_{zz,1}(\pm\rho)\rangle = -1$ condition. In matrix form, the resulting (4×4) system is

$$\begin{pmatrix} 1 & 0 & -\left[\frac{(1+\nu_T)\rho^2}{3}+\frac{(1-\nu_T)a}{4}\right] & -1 \\ \frac{1-\nu_T}{E_T} & -\frac{\nu_A}{E_A} & \frac{(1-\nu_T)}{2G_T}\left(\frac{a}{4}-\frac{\rho^2}{3}\right) & \frac{1}{2G_m} \\ -\frac{2\nu_A}{E_A} & \frac{1}{E_A} & \frac{1}{2G_T}\left[(1-\nu_T)+\frac{2\nu_A E_T\rho^2}{3E_A}\right] & 0 \\ 0 & 1 & \frac{d}{2}+\sum_{i=1}^{\infty}2(-1)^i\left[c_{1i}\left(\frac{c}{s_1^2}-d\right)\frac{I_1(\beta_{1i})}{\beta_{1i}}+c_{2i}\left(\frac{c}{s_2^2}-d\right)\frac{I_1(\beta_{2i})}{\beta_{2i}}\right] & 0 \end{pmatrix}\begin{pmatrix} B_1 \\ B_2 \\ B_3 \\ A_1 \end{pmatrix}=\begin{pmatrix} 0 \\ 0 \\ 0 \\ -1 \end{pmatrix} \tag{81}$$

Once B_3 is known, the remaining constants can be found from $b_{1i} = B_3c_{1i}$, $b_{2i} = B_3c_{2i}$, $a_{0i} = B_3c_{3i}$, and $a_{1i} = B_3c_{4i}$. B_3, besides connecting the two matrix equations, has a physical significance. If the condition in the third row of eqn (81) is substituted into w_1 (eqn (44)) and evaluated at $\zeta = \rho$, we find

$$w_1(\rho) = \rho\frac{B_3(1-\nu_T)}{2G_T}(\xi^2-1) \tag{82}$$

Thus the axial displacement at the end of the fiber or the crack opening displacement is parabolic in ξ with a magnitude proportional to B_3.

We characterize this solution as an *analytical* solution. The solution is expressed as a series of (4×4) linear systems. A patient person could do the algebra and find analytical expressions for all constants in the stress analysis. A more convenient method, however, is to solve the linear systems on a computer. For n Fourier terms, this solution requires solving $(n+1)$ (4×4) systems; such a solution can be done rapidly on any personal computer. We contrast this solution to other stress-transfer solutions which clearly involve numerical methods such as numerically solving an integro-differential equation (Muki and Sternberg (1970)).

Equations (80) and (81) were derived under the assumption that s_1 and s_2 are both real. No difficulties are presented by them being complex, but slightly modified equations are necessary. When s_1 and s_2 are complex they are complex conjugates or $s_2 = s_1^*$. Likewise, β_{1i} and β_{2i} are complex conjugates. Inspection of all the fiber stresses and displacements show that for the stresses and displacements to be real, the constants b_{1i} and b_{2i} and the terms associated with those constants must also be complex conjugates. By resolving all complex terms into their real and imaginary parts, it is a simple matter to write any stress or displacement in terms of the complex number b_{1i} and the complex term associated with b_{1i}. For example, the axial stress in the fiber becomes

$$\sigma_{zz,1} = B_2 + B_3d\xi^2 + \sum_{i=1}^{\infty}\cos k_i\zeta\left[2\Re(b_{1i})\,\Re\left(\left(\frac{c}{s_1^2}-d\right)I_0(\beta_{1i}\xi)\right)-2\Im(b_{1i})\,\Im\left(\left(\frac{c}{s_1^2}-d\right)I_0(\beta_{1i}\xi)\right)\right] \tag{83}$$

where the Bessel functions are now evaluated with complex arguments. All terms involving B_1, B_2, and B_3 are unaffected by whether s_1 and s_2 are real or complex. To find the real and imaginary parts of b_{1i}, we must slightly modify eqn (80). If we use M_{ij} to denote the matrix of constants in eqn (80), the modified equation for complex s_1 and s_2 becomes

$$\begin{pmatrix} 2\Re(M_{11}) & -2\Im(M_{11}) & M_{13} & M_{14} \\ 2\Re(M_{21}) & -2\Im(M_{21}) & M_{23} & M_{24} \\ 2\Re(M_{31}) & -2\Im(M_{31}) & M_{33} & M_{34} \\ 2\Re(M_{41}) & -2\Im(M_{41}) & M_{43} & M_{44} \end{pmatrix}\begin{pmatrix} \Re(b_{1i})/B_3 \\ \Im(b_{1i})/B_3 \\ c_{3i} \\ c_{4i} \end{pmatrix}=\begin{pmatrix} 0 \\ (-1)^i\frac{4(1+\nu_T)}{k_i^2} \\ (-1)^i\frac{4(1-\nu_T)}{2G_Tk_i^2} \\ (-1)^i\frac{8\nu_A(1+\nu_T)}{E_Ak_i^2} \end{pmatrix} \tag{84}$$

After solving this equation, the remaining constants are found from eqn (81). Because of complex constants, the 4–3 element of the matrix in eqn (81) changes to

$$\frac{d}{2}+\sum_{i=1}^{\infty}4(-1)^i\left[\frac{\Re(b_{1i})}{B_3}\Re\left(\left(\frac{c}{s_1^2}-d\right)\frac{I_1(\beta_{1i})}{\beta_{1i}}\right)-\frac{\Im(b_{1i})}{B_3}\Im\left(\left(\frac{c}{s_1^2}-d\right)\frac{I_1(\beta_{1i})}{\beta_{1i}}\right)\right] \tag{85}$$

Finally, identical methods are used to find the constants for problems with isotropic fibers. The resulting equations are

$$\begin{pmatrix} -I_1(k_i) & -2(1-\nu_f)I_1(k_i) - k_iI_0(k_i) & -K_1(k_i) \\ -I_0(k_i) + \frac{I_1(k_i)}{k_i} & -(1-2\nu_f)I_0(k_i) - k_iI_1(k_i) & K_0(k_i) + \frac{K_1(k_i)}{k_i} \\ -\frac{I_1(k_i)}{2G_fk_i} & -\frac{I_0(k_i)}{2G_f} & -\frac{K_1(k_i)}{2G_mk_i} \\ -\left(\frac{I_0(k_i)}{2G_f} + \frac{k_iI_1(k_i)}{D_s}\right) & -\left(\frac{1}{2G_f} + \frac{2(1-\nu_f)}{D_s}\right)k_iI_1(k_i) - \left(\frac{2(1-\nu_f)}{G_f} + \frac{k_i^2}{D_s}\right)I_0(k_i) & \frac{K_0(k_i)}{2G_m} \\ & 2(1-\nu_m)K_1(k_i) - k_iK_0(k_i) & \\ & -(1-2\nu_m)K_0(k_i) + k_iK_1(k_i) & \\ & -\frac{K_0(k_i)}{2G_m} & \\ & \frac{1}{2G_m}\big(k_iK_1(k_i) - 4(1-\nu_m)K_0(k_i)\big) & \end{pmatrix} \begin{pmatrix} c_{1i} \\ c_{2i} \\ c_{3i} \\ c_{4i} \end{pmatrix} = \begin{pmatrix} 0 \\ (-1)^i\frac{4(1+\nu_f)}{k_i^2} \\ (-1)^i\frac{2(1-\nu_f)}{G_fk_i^2} \\ (-1)^i\frac{4\nu_f}{G_fk_i^2} \end{pmatrix} \tag{86}$$

and

$$\begin{pmatrix} 1 & 0 & -\frac{(1+\nu_f)\rho^2}{3} + \frac{\nu_f}{4} & -1 \\ \frac{1-\nu_f}{E_f} & -\frac{\nu_f}{E_f} & -\frac{1}{2G_f}\left(\frac{\nu_f}{4} + \frac{(1-\nu_f)\rho^2}{3}\right) & \frac{1}{2G_m} \\ -\frac{2\nu_f}{E_f} & \frac{1}{E_f} & \frac{1}{2G_f}\left[(1-\nu_f) + \frac{2\nu_f\rho^2}{3}\right] & 0 \\ 0 & 1 & \frac{1}{2} + \sum_{i=1}^{\infty} 2(-1)^i\left[c_{1i}\frac{I_1(k_i)}{k_i} + c_{2i}\left(I_0(k_i) + 2(1-\nu_f)\frac{I_1(k_i)}{k_i}\right)\right] & 0 \end{pmatrix} \begin{pmatrix} B_1 \\ B_2 \\ B_3 \\ A_1 \end{pmatrix} = \begin{pmatrix} 0 \\ 0 \\ 0 \\ -1 \end{pmatrix} \tag{87}$$

RESULTS AND DISCUSSION

Theoretical Results

The above stress analysis satisfies all boundary conditions of the fragmentation test (see Fig. 1) exactly except for the fiber axial stress. Instead of the fiber axial stress being uniformly zero, it is zero only for net fiber stress. We thus expect the solution to be exact except for regions very near the fiber break. Our main interest is in stress transfer at the interface. Because stress transfer into carbon fibers can take 50 fiber diameters (see below), we expect the stress analysis to be virtually exact over the bulk of that stress transfer zone. Any inaccuracies will be confined to the first few fiber diameters of stress transfer.

A complete fragmentation specimen is comprised of numerous fragments. A solution for the entire specimen can be constructed be piecing together solutions for fragments of different lengths. Formally this solution is correct only for periodic fiber breaks. For unequal fragment lengths, there will be a discontinuity in the axial stress in the matrix from one fragment to the next. Thus there is one additional approximation. Despite the axial stress discontinuity, the *net* matrix stress will be continuous from fragment to fragment. Furthermore, the shear stress and displacement continuity conditions between fragments are correctly satisfied.

The stress-analysis problem in Fig. 1 can be viewed as a penny-shaped crack that extends to the boundary between two dissimilar materials. Clearly there should be a stress singularity at the crack tip, at least in the matrix axial stress. The expected singularity is not captured in the present stress analysis. It is missed as a consequence of the fiber stress or the fracture surface being zero in the average instead of uniformly zero. Although there is no mathematical singularity, the series solution converges towards a singularity. As the number of Bessel-Fourier terms increases, the axial stress in the matrix at the crack tip increases. This pseudo-singularity is highly localized at the crack tip. All stresses become independent of the number or Bessel-Fourier terms at positions more than about two fiber diameters from the crack tip.

For a sample calculation, we plot stress transfer from a high modulus (HM) carbon fiber to a room-temperature cured epoxy matrix (see fiber and matrix properties in Table 1). Figure 3 plots the normalized average axial stress in the HM carbon fiber for various values of D_s. For a perfect interface ($D_s = \infty$) the stress transfers back into the fiber in about 30 fiber diameters. As D_s decreases, the stress transfer gets slower. As D_s approaches zero, the interfacial shear stress approaches zero, as it should for a completely disbonded interface. Calculating stresses such as those in Fig. 3 requires including enough terms in the

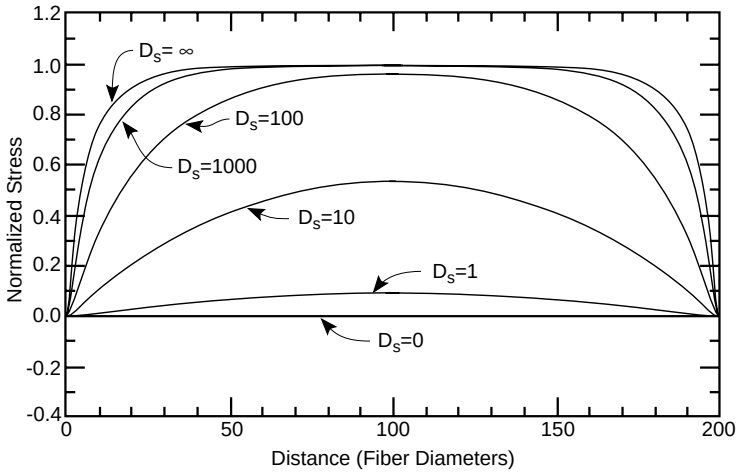

Fig. 3. Sample calculation of the effect of an imperfect interface on the average axial tensile stress in an HM carbon fiber as a function of distance along the fiber for a fiber fragment that is 200 fiber diameters long. All stresses have been normalized to the far-field axial fiber stress of ψ_∞. $D_s = \infty$ is a perfect interface.; $D_s = 0$ is a disbonded interface; intermediate D_s's (in MPa) are imperfect interfaces.

Table I. Thermal and mechanical properties used for the fiber and the matrix

Property	HM Carbon Fibers	Epoxy Matrix
Diameter ($2r_1$) (μm)	7	
Tensile Modulus (E_A or E_m) (GPa)	390	2.6
Transverse Modulus (E_T) (GPa)	14	
Axial Shear Modulus (G_A or G_m) (GPa)	20	0.97
Axial Poisson's Ratio (ν_A or ν_m)	0.20	0.34
Transverse Poisson's Ratio (ν_T)	0.25	
Axial CTE (α_A or α_m) ($10^{-6}/^\circ$C)	-0.36	40
Transverse CTE (α_T) ($10^{-6}/^\circ$C)	18	

Fourier series to get convergence. We found that the average tensile stress converged when the number of terms was on the order of the fragment aspect ratio (ρ). Other components of stress can require more terms but typically never more than $\sim 4\rho$ terms.

The calculated stress transfer rate into a particular matrix is a function of the fiber mechanical properties and of the imperfect interface parameter, D_s. Most previous analyses for stress transfer have been for isotropic fibers. To assess the effect of fiber anisotropy, we considered a series of hypothetical transversely isotropic fibers with mechanical properties

$$E'_A = E_A \tag{88}$$
$$E'_T = E_T + f(E_A - E_T) \tag{89}$$
$$G'_A = G_A + f\left(\frac{E_A}{2(1+\nu_A)} - G_A\right) \tag{90}$$
$$\nu'_A = \nu_A \tag{91}$$
$$\nu'_T = \nu_T + f(\nu_A - \nu_T) \tag{92}$$
$$\alpha'_A = \alpha_A \tag{93}$$
$$\alpha'_T = \alpha_T + f(\alpha_A - \alpha_T) \tag{94}$$

where E_A, E_T, G_A, ν_A, ν_T, α_A, and α_T are the mechanical properties for the HM carbon fiber listed in Table

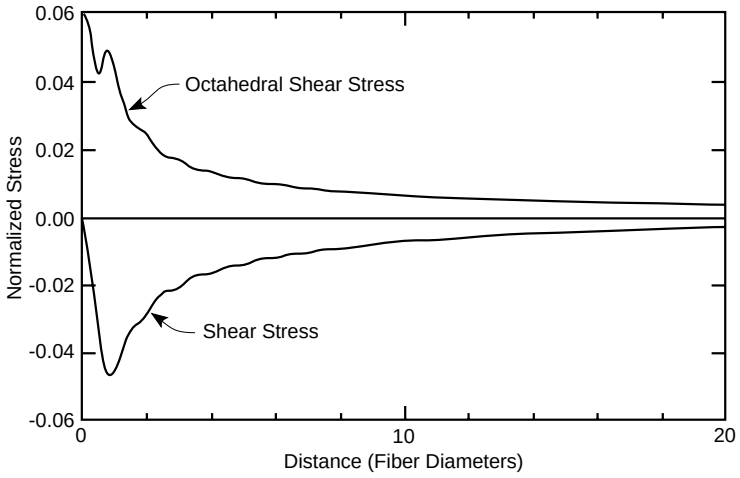

Fig. 4. Sample calculation of the interfacial shear stress and interfacial octahedral shear stress for an HM carbon fiber in an epoxy matrix as a function of distance along the fiber for a fiber fragment that is 200 fiber diameters long. All stresses have been normalized to the far-field axial fiber stress of ψ_∞.

1. As f is varied from 0 to 1, the hypothetical fiber passes smoothly from an HM carbon fiber to an isotopic fiber with $E_f = E_A$, $\nu_f = \nu_A$, and $\alpha_f = \alpha_A$. We found that f had very little influence on the rate of stress transfer. This result suggests that for carbon fibers, fiber anisotropy has little effect of stress transfer. The dominant factor in stress transfer is the ratio of the axial fiber modulus to the matrix modulus. The stress transfer rate decreases as this ratio increases. Although fiber anisotropy has little effect on the stress transfer rate, it has a larger effect on other components of stress (*e.g.*, radial stress at the interface). It is therefore important to include fiber anisotropy when attempting to understand interfacial failure mechanisms

A common interpretation of interfacial damage in fragmentation tests is that it is caused by interfacial shear stresses. These shear stresses are often estimated using one-dimensional elastic models (Cox (1952)) or elasto-plastic models (Kelly and Tyson (1965)). These models misrepresent the interfacial shear stress and predict non-zero shear stress at the fiber ends. In an exact stress analysis, the shear stresses are zero at the fiber end. The analysis in this paper correctly satisfies that boundary condition. A typical plot of interfacial shear stress for a perfect interface is shown in Fig. 4. The shear stress is zero at the fiber break, rapidly reaches a maximum and then decays towards zero. For imperfect interfaces, the maximum decreases and shifts farther away from the fiber break as D_s approaches zero.

The simplistic view of interfacial yielding being caused by interfacial shear stress coupled with the fact of zero shear stress at the fiber ends implies that shear yielding would never occur near the fiber break — an implication that is contrary to observation. The problem with this reasoning is that it ignores the normal stresses. To get a more realistic picture of yielding we consider octahedral shear stress and a von Mises yield criterion instead of only shear stress and a shear-yield criterion. Octahedral shear stress is

$$\tau_{oct} = \frac{1}{3}\sqrt{(\sigma_{rr} - \sigma_{zz})^2 + (\sigma_{rr} - \sigma_{\theta\theta})^2 + (\sigma_{zz} - \sigma_{\theta\theta})^2 + 6\tau_{rz}^2}, \tag{95}$$

As shown in Fig. 4, τ_{oct} is a *maximum* at the fiber ends and decreases away from the fiber ends. Because of normal stresses in the far-field stresses, τ_{oct} does not decay to zero, but to some nonzero, far-field value. The small oscillations near the fiber break are an artifact of the fiber break. When we include enough terms in the Fourier series for convergence (4ρ terms) over most of the fiber, there often remains a very local region near the fiber break that has not converged. As the number of terms increases, τ_{oct} at the fiber end increases. The exact solution has singularities in the normal stresses at the fiber break. This increase in τ_{oct} is a consequence of the Fourier series converging towards the singular stresses. The influence of the singular stress is very local. We found that τ_{oct} converges for distances greater than two fiber diameters from the fiber break.

According to a von Mises yield criterion, the matrix at the interface should yield when $\tau_{oct} \geq \frac{\sqrt{2}}{3}\sigma_y$ where σ_y is the tensile yield stress of the matrix. We claim that τ_{oct} and the von Mises yield criterion give a

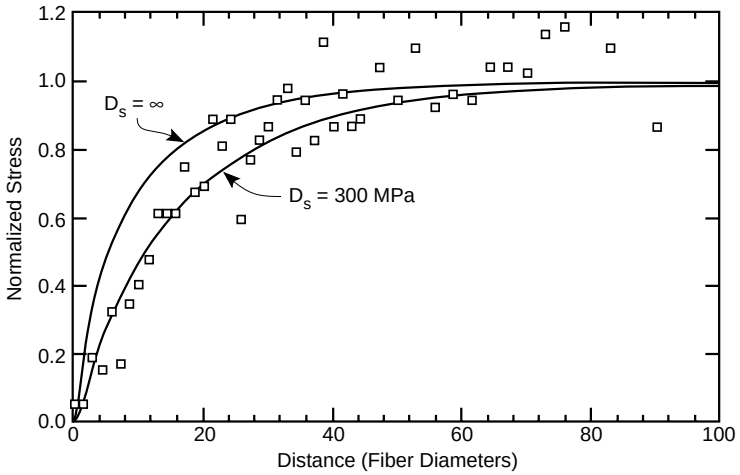

Fig. 5. A comparison of Raman measurements of stress transfer at an applied strain of 0.4% to stress analysis predictions. The $D_s = \infty$ curve is the prediction for a perfect interface. Setting $D_s = 300$ MPa gives a more accurate prediction of the stress transfer process. All stresses have been normalized to the far-field axial fiber stress of ψ_∞.

better picture of the tendency towards interfacial yielding than do models based on shear-lag calculations of interfacial shear stresses. Because of the fiber-end convergence problems, however, one should be cautioned about drawing conclusions based on calculated τ_{oct} very close to the fiber break. Likewise, one should ignore models based on shear-lag or elasto-plastic calculations of the shear stress at the fiber ends.

Comparison to Raman Experiments

Certain Raman bands in carbon fibers shift when the fiber is under stress (Robinson *et al.* (1987)). Several investigators have used this shift to directly measure the stress in a carbon fiber embedded in a matrix (*e.g.*, (Melanitis *et al.* (1992, 1993a, b); Schadler *et al.* (1992))). Here we consider a specific set of experiments on an HM carbon fiber embedded in a room-temperature cured epoxy (Melanitis *et al.* (1993a)). The mechanical properties for the fiber and matrix are given in Table 1. The fibers were embedded in the matrix and the stress in the fiber as a function of distance from the fiber end was measured at several levels of applied strain. Details about the experimental procedures are given in Melanitis *et al.* (1993a). In this section we compare experimental results for fiber stress and interfacial shear stress to stress analysis predictions.

Figure 5 compares the Raman measurements of stress transfer at an applied strain of 0.4% to the predictions of the Bessel-Fourier series stress analysis. We began by assuming a perfect interface. The result in the $D_s = \infty$ curve shows that the predictions agree reasonably well with experimental results. The experimental stress transfer, however, is slightly slower than the predictions. By varying D_s, we found that D_s in the range of 200 MPa to 600 MPa agrees better with experimental results. In Fig. 5, we plot the predicted result for the geometric mean of 200 MPa and 600 MPa or for $D_s = 300$ MPa. We claim that $D_s = 300$ MPa provides a useful measure of the quality of the interface between HM carbon fibers and the epoxy matrix.

Figure 6 shows experimental results at an applied strain of 1.0%. The stress transfer begins slowly, but at about 42 fiber diameters from the end undergoes a discontinuous change in slope. Comparison to Fig. 3 shows that no single value of D_s can predict such a change in stress transfer rate. Instead, we suggest that the high applied strain has caused a damaged zone in the vicinity of the fiber end. The damaged zone could be caused by numerous events such as matrix cracking, matrix yielding, interfacial debonding, or fiber splitting. Whatever the cause of the damage, we claim its effect is to change the effective value of D_s near the fiber end. We thus propose a two-zone model. Within the damaged zone, that extends some distance from the fiber end, the interface is characterized by a low value of D_s. The stresses are found by analysis of a fragment of axial ratio ρ_1 which is equal to the axial ratio of the entire fragment. In the central portion of the fragment, the D_s value is high. The stresses are found by analyzing a fragment of length ρ_2 where ρ_2 is chosen such that the average axial fiber stress is continuous at the edge of the damaged zone. The two-zone

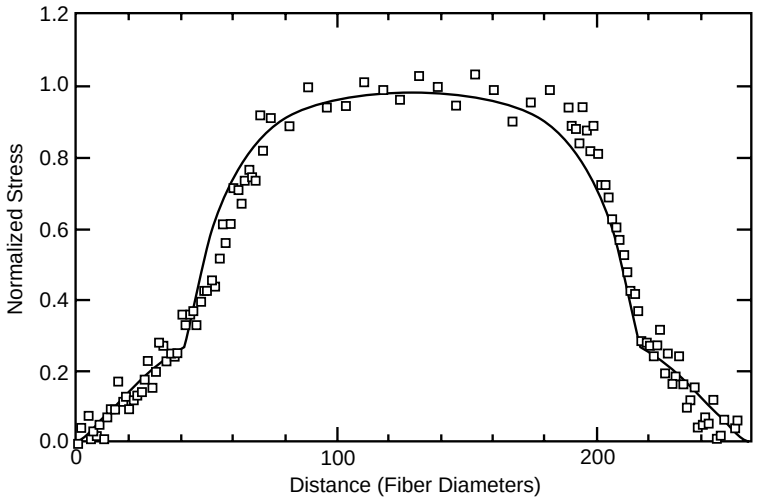

Fig. 6. A comparison of Raman measurements of stress transfer at an applied strain of 1.0% to stress analysis predictions. The predictions are for a two zone model with $D_s = 5$ MPa near the fiber break and $D_s = 300$ MPa in the central portion of the fiber. All stresses have been normalized to the far-field axial fiber stress of ψ_∞.

model is an approximate model because only the average fiber stress is continuous at the junction between the two zones. All other stresses will be discontinuous. We believe the two-zone model still provides a useful model for stress transfer in the presence of a damaged interface.

Figure 6 compares predictions of the two-zone model to experimental results at an applied strain of 1.0%. The D_s value in the center of the fiber represents stress transfer across an undamaged interface. As such, it should be expected to be the same as the D_s value measured over the entire fiber fragment in low-strain experiments. We thus used $D_s = 300$ MPa for the central zone. The best-fit D_s for the damaged zone was $D_s = 5$ MPa. Using these two values of D_s and a damaged zone size of $r_d = 42$ fiber diameters, the analysis agrees well with experimental results. In the damaged zone there is more extensive slip at the interface and a slower rate of stress transfer. This behavior mimics the behavior of stress transfer by friction, although our analysis is not a Coulomb frictional model.

Using the stress analysis to interpret Raman data allows us to measure D_s for the interface between the fiber and the matrix. From the high-strain data, we determined two values of D_s — D_s in the undamaged zone and D_s in the damaged zone. A common practice in fragmentation tests is to continue straining until the fiber fragmentation process ceases. From the average fragment length at the end of the test, the critical fragment length (l_c), a simple elastic-plastic model is used to deduce an interfacial shear strength (Kelly and Tyson (1965)):

$$\tau_{iss} = \frac{\sigma_f(l_c) r_1}{l_c} \tag{96}$$

where $\sigma_f(l_c)$ is the strength of the fiber when tested at a gage length equal to the critical length. There are two reasons for preferring interpretation of fragmentation tests in terms of D_s over interpretation in terms of τ_{iss}. First, τ_{iss} has little or no use in predicting properties of real laminates; it is merely used to compare interfaces. In contrast, Hashin has developed models that allow prediction of laminate properties in terms of D_s (Hashin (1990); Hashin (1990)). Thus by measuring D_s, results from single-fiber tests can give predictive results about the role of the interface in real laminates. Second, τ_{iss} is determined from the highest strain data and thus is determined mostly by D_s is the damaged zone; τ_{iss} is probably unaffected by D_s in the undamaged zone. Among the two D_s values, we claim that D_s in the undamaged zone is the more relevant result. Real laminates never approach fragmentation saturation. To the extent that the interface plays a role in laminate properties, that role is determined by stress transfer over undamaged interfaces. The role of the interface is thus best described by D_s in the undamaged zone. D_s in the undamaged zone is best determined by low strain experiments well below saturation. In contrast, τ_{iss} comes from high-strain, saturation level experiments. These comments cast doubt about the ability of τ_{iss} to give any useful information about the

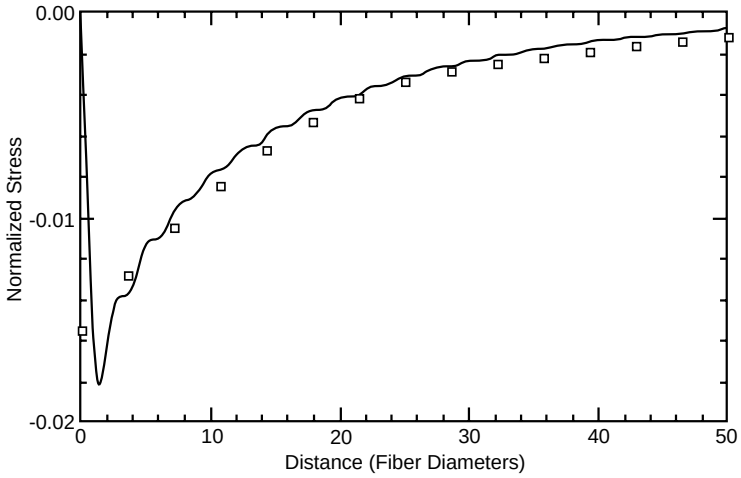

Fig. 7. A comparison of Raman calculations of interfacial shear stress at an applied strain of 0.4% to stress analysis predictions. The predictions are for $D_s = 300$ MPa over the entire fiber. All stresses have been normalized to the far-field axial fiber stress of ψ_∞.

role of the interface in real laminates.

Raman spectroscopy can be used to indirectly determine interfacial shear stresses. By integrating the equation of stress equilibrium for axial loading in axisymmetric stress states, it is easy to show that

$$\tau_{rz}(\xi = 1) = -\frac{r_1}{2}\frac{\partial \langle \sigma_{zz,1} \rangle}{\partial z} \tag{97}$$

where $\langle \sigma_{zz,1} \rangle$ is the average stress in the fiber as a function of z. In Melanitis *et al.* (1993a), this equation was used to deduce interfacial shear stresses. In brief, the experimental data for fiber axial stresses were fit to a cubic spline interpolation and the resulting fit was differentiated to give shear stresses. The shear stresses are not independent experiments, but it is still worthwhile comparing the results to calculated shear stresses. Figures 7 and 8 compare the Raman-determined shear stresses to the calculated shear stresses using the best fit results from Figs. 5 and 6. The low-strain results (Fig. 7) agree well. The Raman results do not show the shear stress dropping to zero at the fiber break because that change is beyond the resolution of the technique. The high-strain results (Fig. 8) also agree well except near the break between the two zones at 42 fiber diameters from the end. The calculated stresses show a discontinuity in shear stresses while the experimental stresses show a smooth peak. We note, however, that the experimental stresses are determined by differentiating a spline fit or "smoothed" curve. Thus, even if a discontinuity or even sharp peak existed, the experimental method would not show it. We therefore regard the peak in the experimental results as consistent with the calculated discontinuity.

A calculation of interfacial octahedral shear stress for the high-strain results suggests a mechanism for the interfacial damage. The octahedral shear stress is low in the damaged zone but increases to a peak at the transition from the damaged zone to the undamaged zone. Figure 9 plots the magnitude of the peak in the octahedral shear stress as a function of the damage zone size for an applied strain of 1.0%. We note that except for very short damage zones, the peak in τ_{oct} occurs away from the fiber break and thus can be calculated without convergence problems. As the damage zone gets larger, the peak in τ_{oct} decreases. For the fits in Figs. 6 and 8, we calculated the damage zone size to be 42 fiber diameters. The peak τ_{oct} for this damage zone size is 48 MPa (see Fig. 9). By a von Mises yield criterion, this τ_{oct} corresponds to an interfacial tensile yield stress of 100 MPa or a shear yield stress of 58 MPa. These are reasonable values for the yield strength of this epoxy matrix. We suggest that the damage zone in these samples was caused by matrix yielding at the fiber/matrix interface. We examined Raman data for other applied strains and found that all could be predicted with a two-zone model. Furthermore, the damage zone size in all experiments was well predicted by a criterion that the maximum τ_{oct} at the break between the two zones is equal to 48 MPa.

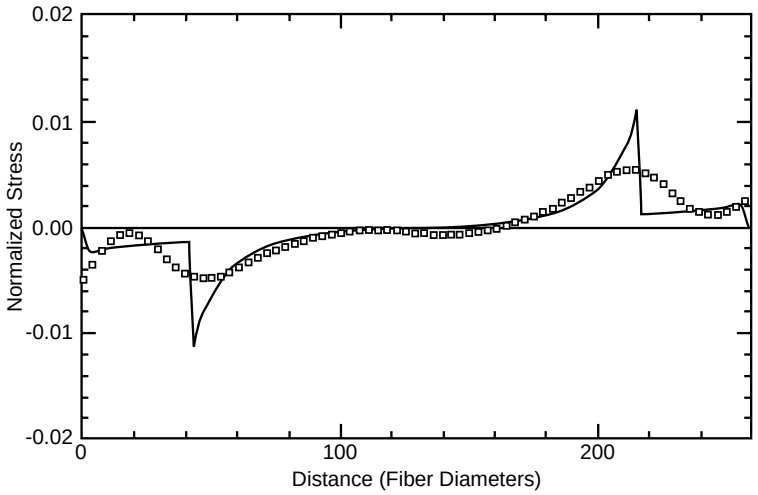

Fig. 8. A comparison of Raman calculations of interfacial shear stress at an applied strain of 0.4% to stress analysis predictions. The predictions are for a two zone model with $D_s = 5$ MPa near the fiber break and $D_s = 300$ MPa in the central portion of the fiber. All stresses have been normalized to the far-field axial fiber stress of ψ_∞.

Strain Energy

We anticipate future work on the fragmentation test being based in fracture mechanics and energy release rate rather than in stress criteria such as interfacial shear stress. The stress state in this paper can be used in fracture mechanics calculations, but first we must integrate the strain energy to get the total strain energy in a fragment with an imperfect interface. The total strain energy in a fiber/matrix fragment is

$$U(\rho) = \int_V \frac{1}{2} \left(\vec{\sigma}_0 + \psi_\infty \vec{\sigma}_p\right) \mathbf{S} \left(\vec{\sigma}_0 + \psi_\infty \vec{\sigma}_p\right) dV \tag{98}$$

$$= \int_V \frac{1}{2} \vec{\sigma}_0 \mathbf{S} \vec{\sigma}_0 dV + \psi_\infty \int_V \vec{\sigma}_0 \mathbf{S} \vec{\sigma}_p dV + \psi_\infty^2 \int_V \frac{1}{2} \vec{\sigma}_p \mathbf{S} \vec{\sigma}_p dV \tag{99}$$

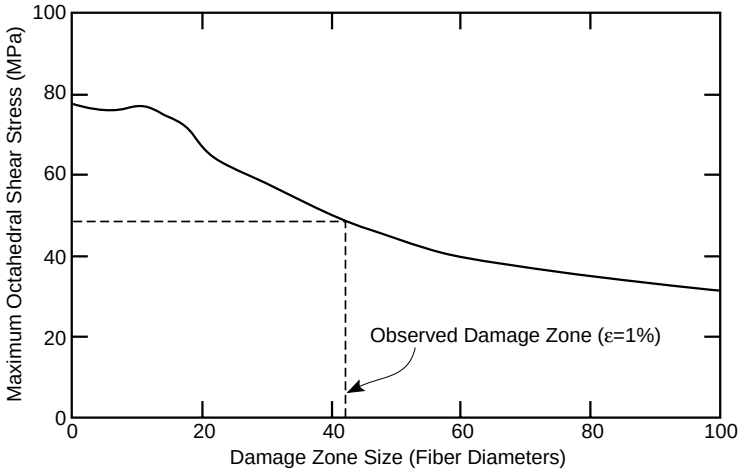

Fig. 9. The peak octahedral shear stress at the break between the two zones in a two-zone model analysis is a function of the size of the damaged zone. The applied strain is 1.0%. $D_s = 5$ MPa in the damaged zone and $D_s = 300$ MPa in the central portion of the fiber. The dashed line shows that the peak octahedral shear stress for the observed damage zone size of 42 fiber diameters when $\varepsilon = 1.0\%$ is 48 MPa.

For now, we treat the perturbation stress, $\vec{\sigma}_p$, as the exact solution to the problem in Fig. 2C. The first term in eqn (99) is the energy due to the far-field stresses. Because of the infinite volume it will be infinite. When these results are used in a fracture mechanics analysis to evaluate energy release rates, the constant infinite term will drop out. We therefore do not need to evaluate it and simply label it as ρU_0 — a constant term that scales with ρ.

The second term in eqn (99) call be evaluated using virtual work. We consider the far-field stresses as having boundary conditions of w_2 constant on the ends of the matrix and $\sigma_{zz,2} = \psi_\infty$ on the ends of the fiber. The perturbation stresses then define a virtual displacement field from the far-field displacements. Thus, by virtual work:

$$\psi_\infty \int_V \vec{\sigma}_0 \mathbf{S} \vec{\sigma}_p dV = 2\psi_\infty \int_{S_f} \psi_\infty r_1 w_1(\rho) dS \tag{100}$$

where S_f is the fiber cross-sectional surface on the top of the fiber. Converting to dimensionless coordinates we get

$$\psi_\infty \int_V \vec{\sigma}_0 \mathbf{S} \vec{\sigma}_p dV = 4\pi r_1^3 \psi_\infty^2 \int_0^1 w_1(\rho) \xi d\xi \tag{101}$$

We split the last term in eqn (99) into integrals over the fiber volume and the matrix volume:

$$\psi_\infty^2 \int_V \frac{1}{2} \vec{\sigma}_p \mathbf{S} \vec{\sigma}_p dV = \frac{\psi_\infty^2}{2} \left[\int_{fiber} \vec{\sigma}_{p,1} \mathbf{S}^{(1)} \vec{\sigma}_{p,1} dV + \int_{matrix} \vec{\sigma}_{p,2} \mathbf{S}^{(2)} \vec{\sigma}_{p,2} dV \right] \tag{102}$$

Using the divergence theorem we can convert these volume integrals to surface integrals giving

$$\psi_\infty^2 \int_V \frac{1}{2} \vec{\sigma}_p \mathbf{S} \vec{\sigma}_p dV = \frac{\psi_\infty^2}{2} \left[\int_{S_{fiber}} \vec{T}_{p,1} \cdot \vec{u}_{p,1} dS + \int_{S_{matrix}} \vec{T}_{p,2} \cdot \vec{u}_{p,2} dS \right] \tag{103}$$

where $\vec{T}_{p,i}$ and $\vec{u}_{p,i}$ are the exact tractions and displacements due to the exact perturbation stresses. The only surfaces that contribute nonzero terms are the top and bottom cross-sections of the fiber and the interfacial surface. The interfacial surface contributes to both the fiber integral and the matrix integral. Evaluating these nonzero terms, doing the hoop integrations, and converting to dimensionless coordinates gives

$$\psi_\infty^2 \int_V \frac{1}{2} \vec{\sigma}_p \mathbf{S} \vec{\sigma}_p dV = \pi r_1^3 \psi_\infty^2 \left[\int_0^1 2 w_1(\rho) \sigma_{zz,1}(\rho) \xi d\xi - \int_{-\rho}^{\rho} \tau_{rz,2}(1) [w] d\zeta \right] \tag{104}$$

where we have assumed the radial displacement discontinuity at the interface is zero ($[u] = 0$)

Combining all terms in eqn (99), using the exact result of $\sigma_{zz,1}(\rho) = -1$, and substituting the imperfect interface condition for $[w]$, the total stain energy in a fiber/matrix fragment reduces to

$$U(\rho) = \rho U_0 + \pi r_1^3 \psi_\infty^2 \left[\int_0^1 2 w_1(\rho) \xi d\xi - \int_{-\rho}^{\rho} \frac{\tau_{rz,2}^2(1)}{D_s} d\zeta \right] \tag{105}$$

This equation is an *exact* expression of strain energy in a fiber/matrix fragment. The first integral is a crack closure integral over the fiber fracture surface. The crack-opening displacement ($\psi_\infty r_1 w_1(\rho)$) is multiplied by the crack-closure force ($\pi r_1^2 \psi_\infty$) and integrated over the fracture surface. The second integral is a closure integral for the imperfect interface effect. If the interface is perfect, this term is ignored. Because an imperfect interface allows the system to slip the total energy is reduced by an imperfect interface.

To evaluate the stain energy using the stress analysis in this paper, we substitute the crack-opening displacement ($w_1(\rho)$, see eqn (82)) and the interfacial shear stress ($\tau_{rz,2}(1)$, see eqn (48)) into eqn (105) and integrate. The result is

$$U(\rho) = \rho \left[U_0 - \pi r_1^3 \psi_\infty^2 \left(\frac{B_3(\rho)(1-\nu_T)}{4G_T} + \frac{S(\rho)}{D_s} \right) \right] \tag{106}$$

where $B_3(\rho)$ is the B_3 constant calculated for a fragment of aspect ratio ρ and

$$\begin{aligned} S(\rho) \quad = \quad & \sum_{i=1}^{\infty} \Big[a_{0i}^2 K_1^2(k_i) - 2 a_{0i} a_{1i} \big(2(1-\nu_m) K_1^2(k_i) - k_i K_0(k_i) K_1(k_i) \big) \\ & + a_{1i}^2 \big(2(1-\nu_m) K_1(k_i) - k_i K_0(k_i) \big)^2 \Big] \end{aligned} \tag{107}$$

The constants in $S(\rho)$ (a_{0i} and a_{1i}) are for a fragment of aspect ratio ρ. Both B_3 and $S(\rho)$ converge as the number of terms in the fiber series increases. The required number of terms is typically $\sim 4\rho$ terms. Because we used the interfacial shear stress in the matrix, the result for isotropic fibers is identical except that ν_T and G_T should be replaced by ν_f and G_f.

For an example energy release rate calculation, imagine a fiber fracture event occurring at the middle of a fiber fragment originally of axial ratio ρ. Because the infinite matrix prevents any external work during the fracture event, the total energy release rate associated with the fiber break is

$$\Delta G = -\frac{\Delta U}{\pi r_1^2} = \rho r_1 \psi_\infty^2 \left[\frac{(1-\nu_T)}{4G_T}\big(B_3(\rho/2) - B_3(\rho)\big) + \frac{S(\rho/2) - S(\rho)}{D_s} \right] \tag{108}$$

(**NOTE ADDED IN REPRINT**: Eq. (108) has a sign error. As explained in J. A. Nairn, *Int. J. Fract.*, in press (1999) (download reprint from `http://www.mse.utah.edu/~nairn/janpubs.html`)), it is not correct to ignore external work. When there are imperfect interfaces, the energy release rate should account for the work of sliding at the fiber/matrix interface. The corrected Eq. (108) should change the the sign of the last term, or change that term to $-(S(\rho/2)-S(\rho))/D_s$. None of the conclusions in this paragraph or in this paper are affected by this sign error.) Note that the infinite terms cancel as expected and ΔG is a well-defined, finite quantity. Some recent experimental fragmentation results for glass fibers in an epoxy matrix show that fiber fracture events do not occur in isolation. Rather, excess energy released by the fiber break causes fiber matrix debonding (Wagner *et al.* (1995)). Our suggested analysis approach for fiber fracture and debonding data is to incorporate a debond zone into the analysis, perhaps using a two-zone model with $D_s = 0$ in the damaged zone, and then to calculate the total energy released for fiber fracture and debonding. We postulate that fragmentation data giving debond size can be interpreted in terms of critical energy release rates for fiber fracture and interfacial fracture. The results in Wagner *et al.* (1995) support this postulate. An energy analysis using the Bessel-Fourier series stress function will be the subject of future work.

Acknowledgments—This work was supported in part by a grant from the Mechanics of Materials program at NSF (CMS-9401772) and in part by a Fulbright Fellowship for one of the authors (J. A. Nairn).

REFERENCES

Bascom, W. D. and Jensen, R. M. (1986). Stress Transfer in Single Fiber/Resin Tensile Tests. *J. Adhes.*, **19**, 219–239.

Bascom, W. D., Yon, K-J., Jensen, R. M. and Cordner, L. (1991). The Adhesion of Carbon Fibers to Thermoset and Thermoplastic Polymers. *J. Adhesion*, **34**, 79–98.

Cox, H. L. (1952). The Elasticity and Strength of Paper and Other Fibrous Materials. *Brit. J. Appl. Phys.*, **3**, 72–79.

Drzal, L. T., Rich, M. J. and Lloyd, P. F. (1983a). Adhesion of Graphite Fibers to Epoxy Matrices: I. The Role of Fiber Surface Treatment. *J. Adhesion*, **16**, 1–30.

Fowler, G. F. and Sinclair, G. B. (1978). The Longitudinal Harmonic Excitation of a Circular Bar Embedded in an Elastic Half-Space. *Int. J. Solids Structures*, **14**, 999–1012.

Fraser, A. A., Ancker, F. H. and DiBenedetto, A. T. (1975). A Computer Modeled Single Filament Technique for Measuring Coupling and Sizing Effects in Fiber Reinforced Composites. *Proc.* 30^{th} *Conf. SPI Reinforced Plastics Div.*, **Section 22-A**, 1–13.

Hashin, Z. (1990). Thermoelastic Properties of Fiber Composites With Imperfect Interface. *Mech. of Materials*, **8**, 333–348.

Hashin, Z. (1990). Composite Materials with Interphase: Thermoelastic and Inelastic Effects. *Inelastic Deformation of Composite Materials*, ed., G. J. Dvorak, Springer-Verlag, New York, 3–34.

Kelly, A. and Tyson, W. R. (1965). Tensile Properties of Fibre-Reinforced Metals: Copper/Tungsten and Copper/Molybdenum. *J. Mech. Phys. Solids*, **13**, 329–350.

Kurtz, R. D. and Pagano, N. J. (1991). Analysis of the Deformation of a Symmetrically-Loaded Fiber Embedded in a Matrix Material. *Composites Engineering*, **1**, 13–27.

Lekhnitski, S. G., (1981).*Theory of an Anisotropic Body*, MIR Publishers, Moscow.

Love, A. E. H., (1944).*A Treatise on the Mathematical Theory of Elasticity*, Dover Publications, New York.

Martin, P. A. (1992). Boundary Integral Equations for the Scattering of Elastic Waves by Elastic Inclusions with Thin Interface Layers. *J. Nondestructive Evaluation*, **11**, 167–174.

Melanitis, N., Galiotis, C., Tetlow, P. L. and Davies, C. K. L. (1992). Interfacial Shear Stress Distribution in Model Composites Part 2: Fragmentation Studies on Carbon Fibre/Epoxy Systems. *J. Comp. Mat.*, **26**, 574–610.

Melanitis, N., Galiotis, C., Tetlow, P. L. and Davies, C. K. L. (1993a). Monitoring the Micromechanics of Reinforcement in Carbon Fibre/Epoxy Resin Systems. *J. Mat. Sci.*, **28**, 1648–1654.

Melanitis, N., Galiotis, C., Tetlow, P. L. and Davies, C. K. L. (1993b). Interfacial Shear Stress Distribution in Model Composites: The Effect of Fiber Modulus. *Composites*, **24**, 459–466.

Muki, R. and Sternberg, E. (1969). On the Diffusion of an Axial Load From an Infinite Cylindrical Bar Embedded in an Elastic Medium. *Int. J. Solids. Structures*, **5**, 587–605.

Muki, R. and Sternberg, E. (1970). Elastostatic Load-Transfer to a Half-Space from a Partially Embedded Axially Loaded Rod. *Int. J. Solids Structures*, **6**, 69–90.

Muki, R. and Sternberg, E. (1971). Load-Absorption by a Discontinuous Filament in a Fiber-Reinforced Composite. *Z. Angew. Math. Phys.*, **22**, 809–824.

Nairn, J. A. (1992). A Variational Mechanics Analysis of the Stresses Around Breaks in Embedded Fibers. *Mech. of Materials*, **13**, 131–154.

Nairn, J. A. and Liu, Y. C. (1996). On the Use of Energy Methods for Interpretation of Results of Single-Fiber Fragmentation Experiments, *Composite Interfaces*, submitted.

Pak, R. Y. S. (1989). On the Flexure of a Partially Embedded Bar Under Lateral Loads. *J. Appl. Mech.*, **56**, 263–269.

Pak, R. Y. S. and Gobert, A. T. (1993). Axisymmetric Problems of a Partially Embedded Rod with Radial Deformation. *Int. J. Solids Structures*, **39**, 1745–1759.

Parnes, R. (1981). Response of an Elastically Embedded Rod Subjected to Periodically Spaced Longitudinal Forces. *Int. J. Solids Structures*, **17**, 891–901.

Penn, L. S. and Bowler, E. R. (1981). A New Approach to Surface Energy Characterization for Adhesive Performance Prediction. *Surf. Interf. Anal.*, **3**, 161–164.

Piggott, M. R., Chua, P. S. and Andison, D. (1985). The Interface Between Glass and Carbon Fibers and Thermosetting Polymers. *Polym. Comp.*, **6**, 242–248.

Rajapakse, R. K. N. D. and Shah, A. H. (1987). On the Longitudinal Harmonic Motion of An Elastic Bar Embedded in an Elastic Half Space. *Int. J. Solids Structures*, **23**, 267–285.

Robinson, I. M., Zakikhani, M., Day, R. J., Young, R. J. and Galiotis, C. (1987). Strain Dependence of the Raman Frequencies for Different Types of Carbon Fibres. *J. Mat. Sci. Lett.*, **6**, 1212–1214.

Schadler, L. S., Laird, C., Melanitis, N., Galiotis, C. and Figueroa, J. C. (1992). Interfacial Studies on Carbon/Thermoplastic Model Composites Using Laser Raman Spectroscopy. *J. Mat. Sci.*, **27**, 1663–1671.

Slaughter, W. S. and Sanders, Jr., J. L. (1991). A Model for the Load-Transfer from an Embedded Fiber to an Elastic Matrix. *Int. J. Solids Structures*, **28**, 1041–1052.

Wadsworth, N. J. and Spilling, I. (1986). Load Transfer from Broken Fibres in Composite Materials. *Br. J. Appl. Phys. (J. Phys. D.)*, **1**, 1049–1058.

Wagner, H. D., Gallis, H. E. and Wiesel, E. (1993). Study of the Interface in Kevlar 49/Epoxy Composite By Means of the Microbond and the Fragmentation Tests: Effect of Materials and Testing Variable. *J. Mat. Sci.*, **28**, 2238–2244.

Wagner, H. D., Nairn, J. A. and Detassis, M. (1995). Toughness of Interfaces from Initial Fiber-Matrix Debonding in a Single Fiber Composite Fragmentation Test. *Applied Composite Materials*, **2**, 107–117.